A steroid-induced osteonecrosis model established using an organ-on-a-chip platform

TENGQI LI[1*], YADI LIU[2*], QINGYU ZHANG[3], WEI SUN[1,4] and YIYANG DONG[2]

[1]Department of Orthopedic Surgery, Peking University China-Japan Friendship School of Clinical Medicine; [2]Department of Bioanalysis, College of Life Science and Technology, Beijing University of Chemical Technology, Beijing 100029; [3]Department of Orthopedics, Shandong Provincial Hospital Affiliated to Shandong First Medical University, Jinan, Shandong 250021; [4]Department of Orthopedic Surgery, China-Japan Friendship Hospital, Beijing 100029, P.R. China

Received April 14, 2020; Accepted September 11, 2020

DOI: 10.3892/etm.2021.10504

Abstract. Bone microvascular endothelial cells (BMECs) constitute the central part of the femoral head's intramural microenvironment network and have an essential role in the development of steroid-induced osteonecrosis of the femoral head. Recently, the rapid development of microfluidic technology has led to innovations in the fields of chemistry, medicine and life sciences. It is now possible to use microfluidics organ-on-a-chip techniques to assess osteonecrosis. In the present study, BMECs were cultured on a microfluidic organ-on-a-chip platform to explore the pathogenesis of femoral-head necrosis. The aim of the present study was to explore the effects of different interventions on BMECs and study the pathogenesis of steroid-induced osteonecrosis through a microfluidic organ-on-a-chip platform. Methods including SU-8 lithography were used to produce a microfluidic organ-on-a-chip and human umbilical vein endothelial cells (HUVECs) were used to test whether it was possible to culture cells on the chip. Subsequently, a set of methods were applied for the isolation, purification, culture and identification of BMECs. Hydroxyapatite (HA) was used for co-culture, dexamethasone was used at different concentrations as an intervention in the cells and icariin was used for protection. BMECs were isolated and cultured from the femoral head obtained following total hip arthroplasty and were then inoculated into the microfluidic organ-on-a-chip for further treatment. In part I of the experiment, HUVECs and BMECs both successfully survived on the chip and a comparison of the growth and morphology was performed. HA and BMECs were then co-cultured for comparison with the control group. The cell growth was observed by confocal microscopy after 24 h. In part II, the effects of different concentrations of glucocorticoid (0.4 or 0.6 mg/ml dexamethasone) and the protection of icariin were evaluated. The morphology of BMECs and the cleaved caspase-3/7 content were observed by immunofluorescence staining and confocal microscopy after 24 h. In the microfluidic organ-on-a-chip, the response of the cells was able to be accurately observed. In part I, at the same concentration of injected cells, BMECs exhibited improved viability compared with HUVECs ($P<0.05$). In addition, it was indicated that HA was not only able to promote the germination and growth of BMECs but also improve the survival of the cells ($P<0.05$). In part II, it was identified that dexamethasone was able to induce BMECs to produce cleaved caspase 3/7; the caspase 3/7 content was significantly higher than that in the blank control group ($P<0.05$) and a dose correlation was observed. Icariin was able to inhibit this process and protect the microvascular structure of BMECs. The content of cleaved caspase 3/7 in the icariin-protected group was significantly lower than that in the group without icariin ($P<0.05$). It was concluded that BMECs are more likely to survive than HUVECs and HA promoted the growth of BMECs on the microfluidic organ-on-a-chip platform. Glucocorticoid caused damage to BMECs through the production of cleaved caspase 3/7, which was observed through the microfluidic organ-on-a-chip platform, and icariin protected BMECs from damage.

Correspondence to: Professor Wei Sun, Department of Orthopedic Surgery, China-Japan Friendship Hospital, 2 Yinghua East Street, Beijing 100029, P.R. China
E-mail: doctor_sunwei@126.com

Professor Yiyang Dong, Department of Bioanalysis, College of Life Science and Technology, Beijing University of Chemical Technology, 15 North Third Ring Road, Beijing 100029, P.R. China
E-mail: yydong@mail.buct.edu.cn

*Contributed equally

Key words: osteonecrosis, bone microvascular endothelial cells, glucocorticoid, microfluidic chip, apoptosis

Introduction

Osteonecrosis of the femoral head is a relatively common and refractory osteoarthropathy. Glucocorticoid is one of the leading causes of non-traumatic necrosis of the femoral head. Its major feature is that the necrosis and regeneration of bone and marrow cells are caused by disorders of the blood supply of the femoral head. Eventually, the femoral head collapses and is deformed and severe hip joint lesions occur (1). The exact pathogenesis of avascular necrosis of the femoral head

remains to be elucidated. There are several hypotheses, including the theory of lipid metabolism disorder, that of intravascular coagulation and that of microvascular injury caused by immune complex deposition. However, the obstacle in the bone tissue blood supply is known to be the fundamental factor of femoral head necrosis. Microcirculation disorder is speculated to be the most common pathway underlying this disease. Bone microvascular endothelial cells (BMECs), involved in the formation of microcirculation, have quickly become a research hotspot. Previous studies have pointed out that BMECs in the necrosed femoral head of patients exhibited different degrees of injury (2). The damage caused by glucocorticoids to BMECs was determined (3,4), while the specific mechanisms remain to be studied.

Microfluidic technologies comprise the control, operation and detection of complex fluids at microscopic sizes. It is able to manipulate the fluids at the submillimeter level. Microfluidic technologies range from simple cell culture chips to organ chips and their application prospect is infinite. Urbaczek *et al* (5) introduced a microfluidic device that is able to simulate blood vessels. This device may be used for cell perfusion culture, as well as cardiovascular and toxicological studies. van Engeland *et al* (6) cultured arterial endothelial and smooth muscle cells in a 3-dimensional microfluidic chip, achieving *in vitro* simulation of arterial wall composition, interaction and mechanical environment. With the development of microfluidic technology, the construction of organ chips has been realized. It is known that the blood-brain barrier is one of the important protective mechanisms of the human body. Through microfluidics, organ-on-a-chip models of the blood-brain barrier are becoming a reality. van der Helm *et al* (7) summarized the recent developments and challenges of this chip model.

The use of multi-disciplinary strategies have now become a trend. The continuous development of microfluidic technology was bound to drive the development of medicine. In the present study, microfluidic technology was used to generate a model of femoral head necrosis by culturing BMEC in a microfluidic organ-on-a-chip. The microfluidic organ-on-a-chip was used to culture BMECs and apply relevant interventions to explore the pathogenesis of osteonecrosis.

Materials and methods

Isolation of BMECs. The femoral head was donated voluntarily by patients undergoing total hip arthroplasty at China-Japan Friendship Hospital (Beijing, China) for femoral neck fractures during November and December 2019. A total of 10 male patients were selected and it was confirmed that their femoral head was normal except from the femoral neck fracture. The patients were aged between 55 and 60 years old and were in a generally good condition. The experiment was approved by the Ethics Committee of China-Japan Friendship Hospital (Beijing, China) and all patients donated their bones voluntarily with written informed consent. Normal cancellous bones from resected femoral heads were cut into 1-2-mm^2 particles and washed three times with PBS to remove the adipose tissue, blood cells and other debris. These bone granules were digested with 5 ml of 0.2% collagenase I (Gibco; Thermo Fisher Scientific, Inc.) for 30 min at 37˚C, followed by trypsinization with 3 ml of 0.25% trypsin-EDTA for 5 min at 37˚C. The process was stopped by adding 2 ml DMEM (Gibco; Thermo Fisher Scientific, Inc.) containing 10% FBS (Shanghai Yeasen Biotechnology Co., Ltd.). The supernatant was filtered through a 70-μM cell strainer and subjected to centrifugation at 107 x g for 5 min at room temperature (RT). The pellet consisted of the harvested microvessels and the cells were resuspended with 80 μl MACS running buffer (Miltenyi Biotec GmbH) and 20 μl of CD31 microbeads (cat. no. 130-091-935; Miltenyi Biotec GmbH). Following incubation for 15 min at 4˚C, the cell suspension was mixed with 400 μl MACS running buffer and added onto a MACS column fixed in the magnetic field. Subsequently, the column was removed and 1 ml DMEM buffer was pipetted onto the column to flush out the labeled cells into a suitable collection tube. Following centrifugation, the pellet was resuspended in 15 ml endothelial cell medium (ECM; ScienCell Research Laboratories, Inc.) and cultivated in a cell incubator at 37˚C with 5% CO_2. After 24 h, the unattached cells were removed by washing with PBS. The BMECs were passaged at 80% confluency and used for subsequent experiments.

Identification of BMECs. The purity of the isolated BMECs was evaluated by immunofluorescence detection of the endothelial markers. The isolated cells were grown on sterile adhesive microscopic slides for 12 h, fixed in 4% paraformaldehyde for 20 min at 4˚C, permeabilized with 0.5% Triton X-100 for 15 min at room temperature, blocked with 10% FBS for 30 min at 37˚C and probed overnight with primary antibody to CD31 (cat. no. ab28364; dilution, 1:300; Abcam) and von Willebrand factor (vWF; cat. no. ab6994; dilution, 1:300; Abcam) at 37˚C. Subsequently, the cells were incubated with secondary antibody conjugated to FITC (cat. no. ab6717; 1:200; Abcam) and Alexa 555 (cat. no. ab150078; 1:200; Abcam) and counterstained with DAPI at RT for 1 h at room temperature. The cell morphology was observed under a fluorescence microscope and 10 fields were randomly selected. The number of immunofluorescence-positive cells was counted and cell purity was calculated.

Microfluidic organ-on-a-chip preparation. The SU-8 photolithography method was used to manufacture a male mold. Silane treatment was performed after the liquid polydimethylsiloxane (PDMS; Sylgard Dow Corning) (the ratio of prepolymer to curing agent was 10:1) was poured on the positive mold, followed by degassing, and after curing at 70˚C for 1 h, and a PDMS microfluidic cover with a thickness of ~2.5 mm was obtained. A 0.5-mm biopsy perforator (Harrick Plasma) was prepared for inlet and outlet. Tape was used to remove dust from the surface, and clean devices and coverslips were plasma-treated (PDC-002; Harrick Plasma) and bonded together. The chip was sterilized with 75% ethanol and ultraviolet light.

Matrix collagen manufacturing and chip injection. A total of 3 mol/l collagen I (Discovery Labware, Inc.) was prepared and placed on ice for later use. HUVECs (BioCoat) and BMECs were trypsinized at 95% confluency and harvested

by centrifugation at 100 x g for 5 min at RT. Cells were collected for counting and the concentration was adjusted to $2.5x10^6$ cells/ml for later use.

Part I [co-culture experiment with hydroxyapatite (HA)]. Three groups were designed: Group A (the HUVEC group), Group B (the control group of BMECs) and group C (the intervention group of BMECs with 0.2% HA), with 3 chips each.

In groups A and B, ECM (ScienCell Research Laboratories, Inc.) and matrix collagen (Discovery Labware, Inc.) were mixed in the equivalent volume of 20 μl each on ice and added to 20 μl cell suspension. Next, 2.5 μl matrix collagen cell mixture was injected into the second channel in the chip. The injection hole was then sealed at both ends of the channel with PDMS pieces to prevent the evaporation of the liquid in the channel. The injected chip was placed in a Petri dish with 1 ml PBS to maintain the moist environment and reduce the evaporation of the liquid in the chip. The assembly was placed in an incubator for 30 min to allow for solidification of the matrix collagen. Subsequently, 5 μl ECM was added to the medium channel of the chip, the injection hole was sealed with PDMS and the chip was placed into the culture dish in the incubator (37˚C, 5% CO_2) for culture. Following incubation for 24 h, cell staining was performed.

In group C, ECM and HA were used to prepare a 0.6% HA suspension. A volume of 20 μl HA suspension was mixed with an equivalent volume of matrix collagen on ice and the same volume of BMEC suspension was added. The remaining steps were the same as above.

Part II (dexamethasone intervention experiment on BMECs). A total of four groups were established: Group D (the blank group), group E (the 0.4 mg/ml dexamethasone intervention group), group F (the 0.6 mg/ml dexamethasone intervention group) and group G (the icariin protection group), with 4 chips in each group (8-10).

The procedure for chip injection was the same as described above. Following a 24-h culture, the growth of the microvascular structure in each chip was observed under the microscope. ECM containing 0.4 or 0.6 mg/ml dexamethasone were prepared using 5 mg/ml dexamethasone (1 ml: 5 mg) mother liquor and ECM. ECM in the medium channel was subsequently replaced with the ECM containing dexamethasone, as aforementioned, for processing. Group D was changed to normal ECM, Group E was altered with the ECM containing 0.4 mg/ml dexamethasone, and group F was changed with the ECM containing 0.6 mg/ml dexamethasone. In group G, the only difference from group F was that medium containing icariin(Solarbio) was first used ($4x10^4$ mol/l) to culture for 24 h, followed by 0.6 mg/ml dexamethasone intervention. Following incubation for 24 h, cell staining was performed.

Caspase 3/7, DAPI and phalloidin staining. To analyze the chips from part I, the medium was aspirated and the chips were washed with PBS twice, followed by fixation with 4% formaldehyde at 4˚C for 10 min and treatment with 0.5% Triton X-100 for 10 min at RT. Subsequently, the chips were probed with 496 nm FITC-labeled phalloidin (cat. no. F432; 300 nM; Invitrogen; Thermo Fisher Scientific, Inc.) at RT for 1 h in the dark. Finally, the nuclei were counterstained with 364 nm DAPI (cat. no. 10236276001; 200 nM; Sigma-Aldrich; Merck KGaA) for 5 min and the film was sealed. Samples could be kept for 3 months at 4˚C in the dark.

In part II, since the fluorescence wavelength of the label for caspase 3/7 (Ex/Em=502/530 nm) was close to that of the 496 nm FITC-labeled phalloidin, a fluorophore with another wavelength, 647 nm FITC-labeled phalloidin, was selected. After the medium was aspirated, the chips were washed with PBS and incubated in 15 μl Caspase-3/7 Green Detection Reagent (cat. no. C10723; 8 μM; Invitrogen; Thermo Fisher Scientific, Inc.) for 1 h to remove extra caspase-3/7 reagent. Subsequently, 4% formaldehyde was used for fixation at 4˚C for 10 min, followed by treatment with 0.5% Triton X-100 for 10 min at RT. Next, 647 nm FITC-labeled phalloidin (cat. no. 40762ES75; 200 nM; Shanghai Yeasen Biotechnology Co., Ltd.) was added and samples were incubated at RT for 1 h in the dark. The nuclei were counterstained with 364 nm DAPI for 5 min prior to sealing and storing at 4˚C in the dark.

Cell imaging detection. Staining images were captured by a confocal microscope using the 10-fold lens or 40-fold oil lens. An interface with optimal cell morphology, clear staining and no bubble interference was selected. The number of cells was compared by counting the number of nuclei, the area coverage of microfilament skeletons was determined to compare the growth status of the cells and the area coverage of cleaved caspase-3/7 was determined to compare the cell damage among the groups. The imaging data were analyzed using ImageJ software (https://imagej.nih.gov/ij/) (11,12).

Statistical analysis. Values are expressed as the mean ± standard deviation. All data were analyzed by SPSS 20.0 statistical software (IBM Corp.). Differences among multiple groups were analyzed by one-way ANOVA followed by Tukey's post-hoc test. $P<0.05$ was considered to indicate a statistically significant difference.

Results

Cell culture and chip preparation. A microfluidic organ-on-a-chip and schematic diagram of the top view is presented in Fig. 1A. It contained four channels, including those for infusion of drugs and cell microchannels, infusion of VEGF-containing medium microchannels and an ECM simulation region. The internal size specification of each channel was identical and a micropillar structure separated the channels. The cells were able to be inoculated into either channel and the medium was injected into adjacent channels. In the identification of BMECs, under a fluorescence microscope, immunofluorescence demonstrated high expression of CD31 and vWF (Fig. 1B).

Fig. 1C is the cell image acquired by an ordinary optical microscope (magnification, x100). The left is the BMECs cultured in ordinary Petri dishes, and the right is the BMECs inoculated into the chip. In Petri dishes, most cells clustered together, and there are few connective structures between cells. And the microscopic connection between BMECs in the chip was increased. The structure of the cells, with the microscopic connections, with similar vascular structures, was different from the common culture model.

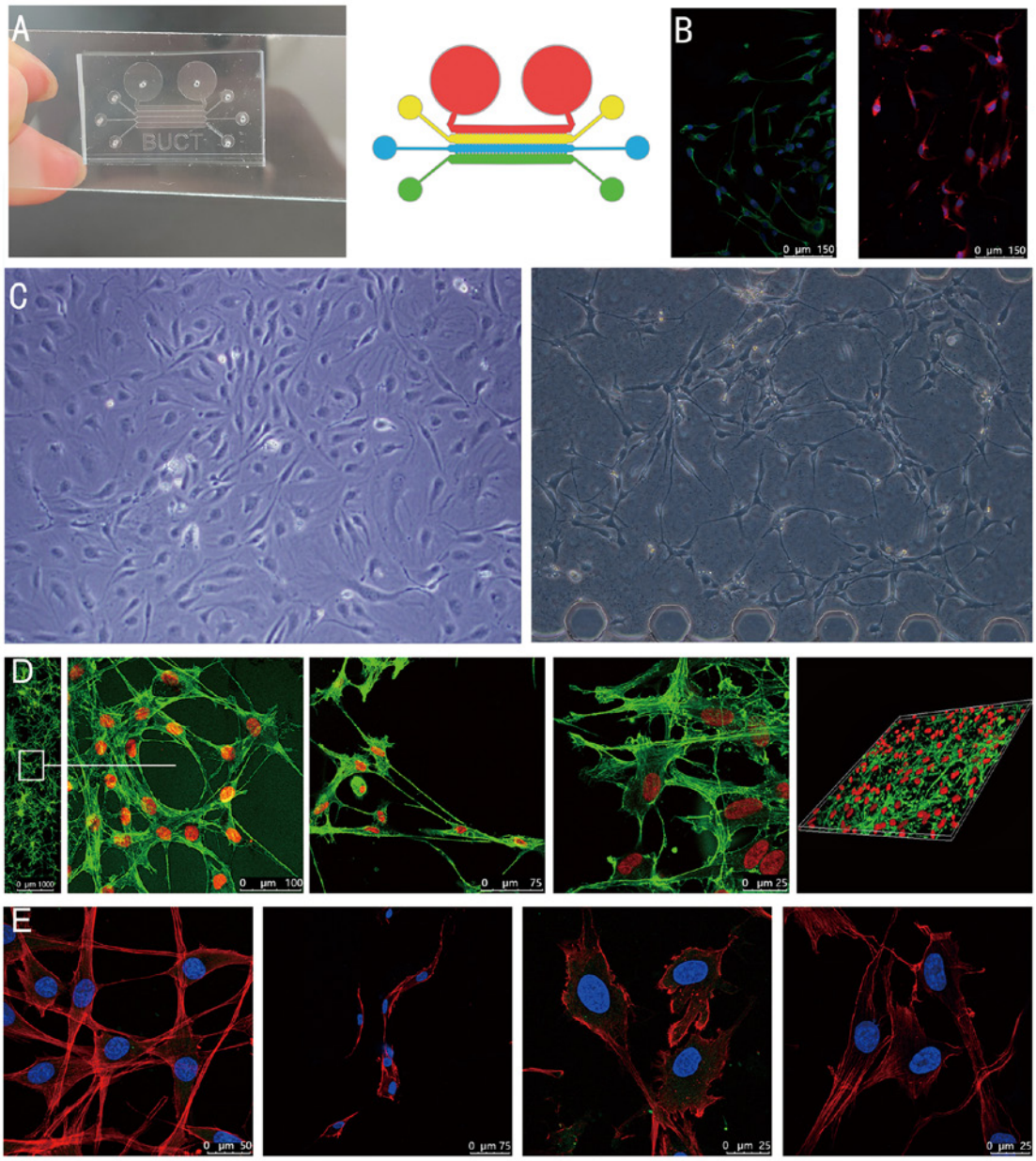

Figure 1. (A) Microfluidic chip and schematic diagram of the top view. Four different coloured areas represent its four channels. (B) Identification of bone microvascular endothelial cells and immunofluorescence staining revealed high expression of von Willebrand factor (green) on the left side and CD31 (red) on the right side, and both nuclei were counterstained with DAPI (scale bars, 150 μm). (C) Ordinary optical microscope images. The left is taken from ordinary Petri dishes, and the right is from the microfluidic chip (Magnification, x100). (D) Confocal microscopy images. From left to right, the first image is the microfluidic chip channel panorama taken by a confocal microscope using the 10-fold lens and a partial enlargement (scale bar in magnified window, 100 μm). The second and third images are high-resolution images obtained by a confocal microscope using the 40-fold oil lens (scale bars, 75 and 25 μm, respectively). The last image is a laminated and reconstructed solid image obtained using confocal microscopy. (E) Cells in high-definition close-up (scale bars, 50, 75, 25 and 25 μm, respectively, from left to right).

Fig. 1D and E present high-resolution images of cells captured with a confocal microscope following cell death. In Fig. 1D, from left to right, the first image is a microfluidic chip channel panorama obtained by confocal microscopy using the 10-fold lens and a partial enlargement. The second and third images are high-resolution images acquired by a confocal microscope using the 40-fold oil lens. The last image is a laminated and reconstructed solid image obtained using confocal microscopy. Fig. 1E presents selected cells in high-definition close-up during the experiment in part II. Through these high-definition images, the microscopic morphology and structure of the cells, the microfilament connections between cells and the morphology of the nucleus can be observed more clearly.

Part I (co-culture experiment of HA). The images and data were analyzed following collection (Fig. 2). The results were as follows: The number of cells that survived in group B was significantly higher than that in group A ($P<0.05$), and that in group C was also significantly higher compared with that in group B ($P<0.05$). In addition, the area coverage percentage of the microfilament cytoskeleton in group C was significantly higher than that in group B ($P<0.05$). Morphologically, several microfilament connections between cells and circular

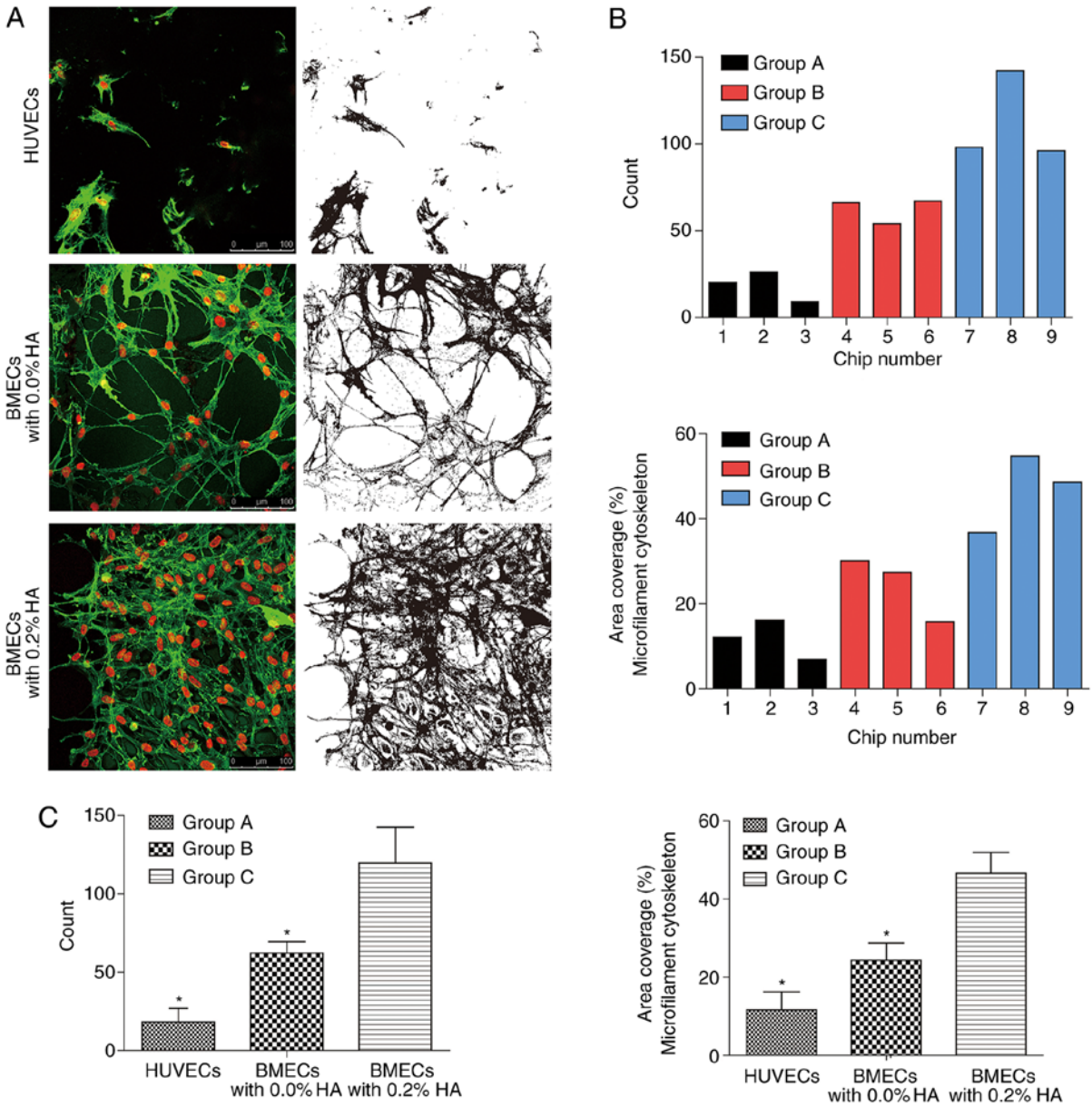

Figure 2. Results of Part I. (A) Confocal microscopy image of cells in the different groups. Green represents phalloidin and the red represents DAPI (changed from blue for better visibility; 40-fold oil lens; scale bars, 100 μm). (B) Quantitative analysis for each individual chip in this part was performed using ImageJ software: Upper panel, cell count per field; lower panel: area coverage of microfilament cytoskeleton (%). (C) Overall statistical analysis for this part; the cell number and the area coverage of the cytoskeleton of group C were significantly higher compared with those of the other two groups. *P<0.05 vs. group C. BMECs, bone microvascular endothelial cells; HUVEC, human umbilical vein endothelial cells; HA, hydroxyapatite.

structures that resemble blood vessels were observed, particularly in group B. In addition, BMECs grew more vigorously compared with HUVECs, and BMECs co-cultured with HA grew most vigorously.

Part II (dexamethasone intervention experiment of BMECs). The images and data for the experimental Part II are presented in Fig. 3. The results demonstrated that there was no significant difference in the number of cells between groups D, E and G (P>0.05); however, the number of cells in group F was significantly higher than that in groups D and E (P<0.05).

In addition, a significant difference was detected in the content of cleaved caspase-3/7. The production of cleaved caspase-3/7 was evident in group F and was significantly higher than that in all other groups (P<0.05). There was no significant difference in the content of cleaved caspase-3/7 between groups E and G (P>0.05). Additionally, the content of cleaved caspase-3/7 was significantly lower compared with all other groups (P<0.05).

Furthermore, the area coverage of the microfilament cytoskeleton in group F was significantly lower than that in all other groups (P<0.05). There was no significant difference among the other three groups (P>0.05).

In addition to the quantitative results, there were numerous observations regarding morphology and cellular location of proteins. First, the localization of cleaved caspase-3/7 was distinct in the cell, and these proteins were located around the nucleus. Furthermore, in group F, the morphological structure of the cells was altered, the

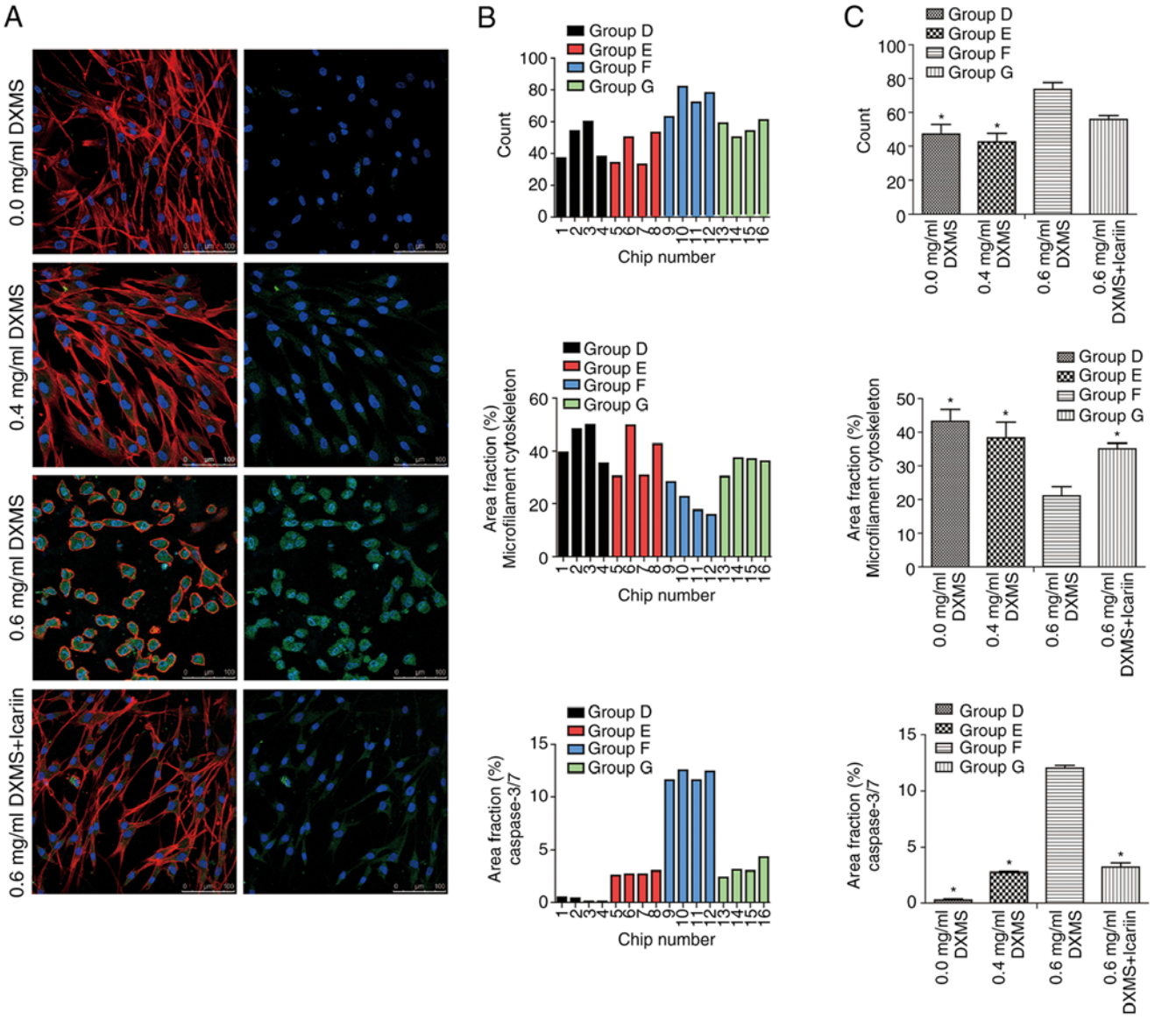

Figure 3. Result of Part II. (A) Immunofluorescent confocal microscopy images obtained using the 40-fold oil lens. The two images are from the same field of view and the second image was obtained with the red channel turned off for easy observation. Green represents caspase-3/7, red indicates phalloidin and blue represents DAPI (scale bar, 100 μm). (B) Quantitative analysis for each individual chip in this part was performed using ImageJ software. (C) Overall statistical analysis for this part; the cell count per field in group F was significantly higher compared with that in groups D and E. The area coverage of the cytoskeleton in group F was significantly lower compared with that in the other groups and the content of caspase-3/7 in group F was significantly higher compared with that in the other groups. *P<0.05 vs. group F. DXMS, dexamethasone.

microfilament structure between the cells had disappeared and the cells changed from elongated to a round shape. Finally, the cell morphology in the other three groups was similar.

Discussion

HA has been widely used in bone tissue simulation for a long time, due to its similar structure and osteoinductive characteristics. It has also been recognized as the best bone graft material. Bones consist mainly of collagen and calcium phosphate (Cap) minerals and Cap minerals are similar to HA minerals in composition and structure. The brittle texture of HA limits its application as a load-bearing material, and therefore, it requires to be synthesized with other polymers to improve its mechanical properties (13,14). Jusoh *et al* (15) simulated the bone structure with HA in a microfluidic chip, using HA to induce the growth of HUVECs across channels. The results indicated that the group treated with 0.2% HA exhibited the best endothelial cell morphology and the most reliable vasculature-forming ability. Based on the above experience, in addition to the traditional cultivation of HUVECs, BMECs extracted and cultured by our group were used for a similar experiment and co-culture was also performed in the microfluidic organ-on-a-chip. It was identified that the viability of HUVECs in the chip was relatively weak. At the same concentration of injected cells, HUVECs growth was not as vigorous as BMECs's. Although there were also microfilaments between HUVECs, they did not form a structure similar to blood vessels as BMECs in Group B did. This may be due to the limited vitality of the purchased HUVECs. As BMECs are primary cells extracted

from cancellous bone, their vitality may be higher than that of frozen HUVECs. In the co-culture group, the microfilament connections between cells were significantly increased ($P<0.05$) and the cells were dense. The results were similar to those of the study by Jusoh *et al* (15). In addition, the number of BMECs co-cultured with HA also increased significantly ($P<0.05$). Considering the space in the channel and the concentration of injected cells, the physical structure of HA may provide a more favorable growth environment for cells. HA was considered to be able to keep BMECs alive rather than to promote cell division. The reason for the higher number of cells in the HA group was that more cells in the control group died. In the presence of HA, Whisler *et al* (16) also co-cultured the HUVECs and pulmonary fibroblasts in a microfluidic chip and concluded that pulmonary fibroblasts were useful for maintaining the morphology of vascular cells and prolonging the survival time of vascular cells in the chip for up to 4 days. A notable phenomenon was identified in the present study as in that the morphological structure of the HUVECs being not as healthy as that of the cells in the study by Whisler *et al* (16), and no vascular lumen was observed as it was in their study. However, the morphological structure of BMECs was similar to that of the HUVECs in the study by Whisler *et al* (16), particularly in Group B. The cells formed a structure similar to that of the circular lumen, which is similar to the image published in the literature, and even the panoramic image. Given that both BMECs and HUVECs are essentially vascular endothelial cells, just derived from different parts of the human body, it is understandable that their morphology and structure were similar.

In the present study, although there was not a very typical three-dimensional structure, fluorescence staining indicated that the cells were connected by microfilaments in the matrix collagen. Furthermore, the morphology was somewhat different from that of cells in ordinary Petri dishes. The major characteristics of the present microfluidic organ-on-a-chip were as follows: i) Fluidity. The cells were suspended in the matrix collagen, were able to move slightly and grew in all directions, not limited to a plane. ii) Independence. The microfluidic organ-on-a-chip had four channels, each of which was able to be used for liquid injection. However, due to the effect of surface tension of the liquids, there would be no leakage between the empty and liquid channels. iii) Feasibility of intervention. Adjacent channels were available for the addition of different drugs and other interventions, as well as for changes in the medium or the final addition required for fluorescent staining.

Apoptosis is programmed cell death regulated by apoptosis-associated genes in order to maintain the stability and integrity of the genome. Apoptosis involves the activation, expression and regulation of a series of genes and it differs from cell necrosis in morphology and biochemistry. The caspase family is a cysteine protease system with a specific aspartic cysteine that is a key player in apoptosis (17,18). To date, ≥14 caspase members have been implicated in apoptosis in mammals. The stimulation of various proteases also activates caspase-induced apoptosis through different pathways. However, mammalian cell apoptosis is effectuated via caspase-3. The increased expression and stimulation of caspase-3 is a central link in the early initiation of the apoptotic signaling pathway and is also one of the vital proteases involved in the regulation and execution of apoptosis (19).

Microfluidic organ-on-a-chip provided a new environment for the growth of cells. In the chip, it was indicated that the microfilaments between cells not only increased but it was also easier for the cells to form tubular structures between each other. In some areas, the formation of tubular structures between only three cells was observed. In petri dishes, cells attach themselves to the flat surface of the dish and could only grow in the directions on one surface to touch the surrounding cells. In the chip, cells could grow in all directions in a three-dimensional environment, touching cells all around rather than being confined to a single plane. This increased the probability of contact between cells and made it easier for them to form tubular structures. The chip, combined with confocal microscopy, provides high-resolution morphological results for cellular experiments. In the experiment of the present study, the appearance of apoptotic proteins (caspase-3/7) was able to be directly observed in the microfluidic organ-on-a-chip and it was also identified that the glucocorticoid caused the apoptosis of BMECs. The comparison not only revealed a significant increase in the cleaved caspase-3/7 content ($P<0.05$), but its release from the nucleus was also directly visible to the naked eye. The glucocorticoid-treated BMECs produced more cleaved caspase-3/7, and with the increase of the glucocorticoid concentration, cleaved caspase-3/7 also increased significantly ($P<0.05$). Particularly in the high-concentration glucocorticoid intervention group, in addition to high expression of cleaved caspase-3/7, BMECs also exhibited obvious atrophy in morphology; the proportional area of the whole cytoskeleton was significantly smaller than that of the other three groups ($P<0.05$). The microfilaments all disappeared, the cells became round, and the whole cell appeared to be on the verge of death. Furthermore, the number of cells in this group increased significantly compared with that in the other groups ($P<0.05$). Combined with cell morphology, high-concentration glucocorticoid resulted in cell atrophy and volume reduction; therefore, the number of cells increased in the same field area. Furthermore, the concentration of dexamethasone used in the present study was selected according to our previous experiment (8-10). The concentration of drug used in the present study was slightly higher than the previously used concentration of 0.1 or 0.2 mg/ml for two main reasons. First, different from using a culture dish, the ECM containing dexamethasone was added to the chip through channels and the volume of the two channels of the ECM and the cell directly diluted the concentration of dexamethasone by 50%. Furthermore, in an ordinary culture dish, cells are in direct contact with dexamethasone in the ECM, while in the microfluidic chip, cells are suspended in the matrix collagen and dexamethasone is required to permeate through the matrix collagen to be in contact with the cells. Therefore, a higher concentration is required to achieve the same effect as in an ordinary culture dish. In addition, the concentrations of 0.4 and 0.6 mg/ml used in the present study were low for the human body but were sufficiently high to be lethal for the cells *in vitro*. The purpose of the present study was to investigate the mechanism of cell damage in order to guide clinical treatment, and it is difficult to directly calculate the

appropriate clinical drug concentration through cell experiments. Therefore, further investigation may be required to determine a more appropriate dose to be used in the clinic.

Several mechanisms are able to induce apoptosis, and it has been well observed that glucocorticoid induces apoptosis of BMECs (10). However, specific mechanisms remain elusive and should be clarified to improve treatment approaches. It has been speculated that oxidative stress is the primary mechanism to trigger apoptosis. In the case of oxidative stress, excessive reactive oxygen species (ROS) cause cell damage and the body forms a complex oxidative stress response system against ROS damage (20). Tang *et al* (21) reported that polychlorinated biphenyl 118 is able to elevate the ROS levels in HUVECs to initiate apoptosis. In addition to directly triggering apoptosis, ROS accumulation may activate a series of signaling pathways, leading to the dysregulation of apoptosis and excessive cell death. Excessive apoptosis leads to autoimmune diseases and inflammation, which are associated with various acute and chronic diseases (22). ROS generated by oxidative stress causes cell damage, which in turn leads to excessive accumulation of ROS. The accumulated ROS induces excessive apoptosis, which further aggravates damage (23).

Icariin is a flavonoid compound that has biological activities, including immune regulation, anti-tumor, anti-aging and cardiovascular effects. Previously, Zhao *et al* (10) studied the protective effect of icariin on glucocorticoid-treated BMECs. Using the TUNEL method, it was identified that icariin inhibited apoptosis of BMECs by glucocorticoids. In addition, Hu *et al* (24) revealed that icariin prevented the injury and apoptosis of HUVECs by regulating caspase-3 and B-cell lymphoma 2. In the icariin-protected group of the present study, it was observed that although a considerable amount of cleaved caspase-3/7 was produced in the cytoplasm, the content was significantly lower than that in the high-concentration glucocorticoid group ($P<0.05$). In addition, the microfilamentous structural connections between the cells were similar to those in the other groups and the cells did not shrink. Furthermore, the area of the whole cytoskeleton was not significantly different compared with that in the blank group ($P>0.05$). This suggested that advanced protection with icariin reduced the damaging effect of glucocorticoid on the cells and protected the microvascular structure. Chen *et al* (25) investigated the protective mechanism of icariin by using endothelial cells from rat femurs. It was identified that icariin had a protective effect on the high glucose-induced endothelial cells by inhibiting p38/cyclic AMP response element-binding protein and activating the Akt/eNOS/NO pathway. Xiao *et al* (26) also reported that icariin decreased ROS production in HUVECs. Wang *et al* (27) summarized the various functions of icariin, including attenuation of hydrogen peroxide impairment, improvement of cell viability, inhibition of cell apoptosis and increase of superoxide dismutase and glutathione peroxidase activity. It may be suggested that further studies are required in the future to demonstrate the inhibitory effect of icariin on cell apoptosis, as well as its cellular protective mechanisms.

The advantage of the microfluidic organ-on-a-chip used in the present study was that it was easy to operate. Through adjacent channels, it was possible to add various substances used to directly stain the cells *in situ* and target the exact position in the cell. As for caspase-3, in the present experiment, it is well known that western blot analysis is able to analyze intracellular proteins and detect the types and content of proteins. A microfluidic organ-on-a-chip can be an excellent supplement to western blot analysis. The target protein may be observed directly with the naked eye by staining, and at the same time, a simple content comparison may be performed. It is also possible to determine whether the location of the target protein is consistent with the theory and it provides a high-resolution morphological visualization for cell experiments.

In conclusion, from the perspective of morphology, BMECs were more likely to survive compared with HUVECs in the chip used in the present study and HA was able to promote the growth of BMECs through the microfluidic platform. Glucocorticoids were able to damage cells through the production of cleaved caspase 3/7 and icariin protected the cells to a certain extent and reduced the damage of glucocorticoids to cells.

Acknowledgements

Not applicable.

Funding

This study was supported by the Beijing Natural Science Foundation (grant no. 7182146), the Biomedical Translational Engineering Research Center of BUCT-CJFH (grant no. RZ2020-02) and the National Natural Science Foundation of China (grant nos. 81672236, 81802224 and 81871830).

Availability of data and materials

The datasets used and/or analyzed during the current study are available from the corresponding author on reasonable request.

Authors' contributions

YD and WS were responsible for designing and directing the whole experiment. TL was responsible for performing the cell experiment, collecting the data and writing the initial manuscript. YL was responsible for designing and making microfluidic chips, and writing the initial manuscript. QZ was responsible for isolating cells, analyzing the data, and reviewing the manuscript. TL, YL, QZ, YD and WS confirmed the authenticity of all the raw data. All authors read and approved the final manuscript.

Ethics approval and consent to participate

The experiment was approved by the Ethics Committee of China-Japan Friendship Hospital (Beijing, China) and all patients donated voluntarily with written informed consent.

Patient consent for publication

The patients provided consent for publication.

Competing interests

The authors declare they have no competing interests.

References

1. Zhao D, Liu Y, Ma C, Gu G and Han DF: A mini review: Stem cell therapy for osteonecrosis of the femoral head and pharmacological aspects. Curr Pharm Des 25: 1099-1104, 2019.
2. Maruyama M, Lin T, Pan CC, Moeinzadeh S, Takagi M, Yang YP and Goodman SB: Cell-Based and scaffold-based therapies for joint preservation in early-stage osteonecrosis of the femoral head: A review of basic research. JBJS Rev 7: e5, 2019.
3. Yu Q, Guo W, Shen J and Lv Y: Effect of glucocorticoids on lncRNA and mRNA expression profiles of the bone microcirculatory endothelial cells from femur head of Homo sapiens. Genom Data 4: 140-142, 2015.
4. Yu QS, Guo WS, Cheng LM, Lu YF, Shen JY and Li P: Glucocorticoids significantly influence the transcriptome of bone microvascular endothelial cells of human femoral head. Chin Med J (Engl) 128: 1956-1963, 2015.
5. Urbaczek AC, Leão PAGC, Souza FZR, Afonso A, Vieira Alberice J, Cappelini LTD, Carlos IZ and Carrilho E: Endothelial cell culture under perfusion on A polyester-toner microfluidic device. Sci Rep 7: 10466, 2017.
6. van Engeland NCA, Pollet AMAO, den Toonder JMJ, Bouten CVC, Stassen OMJA and Sahlgren CM: A biomimetic microfluidic model to study signalling between endothelial and vascular smooth muscle cells under hemodynamic conditions. Lab Chip 18: 1607-1620, 2018.
7. van der Helm MW, van der Meer AD, Eijkel JC, van den Berg A and Segerink LI: Microfluidic organ-on-chip technology for blood-brain barrier research. Tissue Barriers 4: e1142493, 2016.
8. Yu Q, Guo W, Cheng L, Lu Y and Li P: Preliminary study of impact of steroids on expression profile and transcriptome of bone microvascular endothelial cells. Zhonghua Yi Xue Za Zhi 94: 3817-3820, 2014 (In Chinese).
9. Zhang Q, Gao F, Cheng L, Liu L, Sun W and Li Z: Effects of icariin on autophagy and exosome production of bone microvascular endothelial cells. Zhongguo Xiu Fu Chong Jian Wai Ke Za Zhi 33: 568-577, 2019 (In Chinese).
10. Zhao DY, Yu QS, Guo WS and Cheng LM: Effect of icariin on the proteomic expression profile of bone microvascular endothelial cells of human femoral head against steroids-induced lesion. Zhonghua Yi Xue Za Zhi 96: 1026-1030, 2016 (In Chinese).
11. Wang X, Sun Q and Pei J: Microfluidic-Based 3D engineered microvascular networks and their applications in vascularized microtumor models. Micromachines (Basel) 9: 493, 2018.
12. Zhang Z, Chen YC, Cheng YH, Luan Y and Yoon E: Microfluidics 3D gel-island chip for single cell isolation and lineage-dependent drug responses study. Lab Chip 16: 2504-2512, 2016.
13. Rh Owen G, Dard M and Larjava H: Hydoxyapatite/beta-tricalcium phosphate biphasic ceramics as regenerative material for the repair of complex bone defects. J Biomed Mater Res B Appl Biomater 106: 2493-2512, 2018.
14. Ramesh N, Moratti SC and Dias GJ: Hydroxyapatite-polymer biocomposites for bone regeneration: A review of current trends. J Biomed Mater Res B Appl Biomater 106: 2046-2057, 2018.
15. Jusoh N, Oh S, Kim S, Kim J and Jeon NL: Microfluidic vascularized bone tissue model with hydroxyapatite-incorporated extracellular matrix. Lab Chip 15: 3984-3988, 2015.
16. Whisler JA, Chen MB and Kamm RD: Control of perfusable microvascular network morphology using a multiculture microfluidic system. Tissue Eng Part C Methods 20: 543-552, 2014.
17. Chen P, Zhang H, Zhang Q, Zhou W, Deng Y, Hu X and Zhang L: Basic Fibroblast growth factor reduces permeability and apoptosis of human brain microvascular endothelial cells in response to oxygen and glucose deprivation followed by reoxygenation via the fibroblast growth factor receptor 1 (FGFR1)/ERK pathway. Med Sci Monit 25: 7191-7201, 2019.
18. Chen X, Jiang Y, Wang J, Liu Y, Xiao M, Song C, Bai Y, Yinuo Han N and Han F: Synapse impairment associated with enhanced apoptosis in post-traumatic stress disorder. Synapse 74: e22134, 2020.
19. Gao X, Zhang Y, Zhang R, Zhao Z, Zhang H, Wu J, Shen W and Zhong M: Cyclin-dependent kinase 1 disruption inhibits angiogenesis by inducing cell cycle arrest and apoptosis. Exp Ther Med 18: 3062-3070, 2019.
20. Yuan W, Chang H, Liu X, Wang S, Liu H and Xuan H: Brazilian green propolis inhibits Ox-LDL-Stimulated Oxidative Stress In Human Umbilical Vein Endothelial Cells Partly through PI3K/Akt/mTOR-Mediated Nrf2/HO-1 Pathway. Evid Based Complement Alternat Med 2019: 5789574, 2019.
21. Tang L, Cheng JN, Long Y, He XM, Liang GN, Tang XP, Jiang CX and Chen F: PCB 118-induced endothelial cell apoptosis is partially mediated by excessive ROS production. Toxicol Mech Methods 27: 394-399, 2017.
22. Munoz M, López-Oliva ME, Rodríguez C, Martínez MP, Sáenz-Medina J, Sánchez A, Climent B, Benedito S, García-Sacristán A, Rivera L, *et al*: Differential contribution of Nox1, Nox2 and Nox4 to kidney vascular oxidative stress and endothelial dysfunction in obesity. Redox Biol 28: 101330, 2020.
23. Fernandez-Bertolez N, Costa C, Bessa MJ, Park M, Carriere M, Dussert F, Teixeira JP, Pásaro E, Laffon B and Valdiglesias V: Assessment of oxidative damage induced by iron oxide nanoparticles on different nervous system cells. Mutat Res 845: 402989, 2019.
24. Hu Y, Li H, Liu K, Zhang Y, Ren L and Fan Z: Protective effects of icariin on human vascular endothelial cells induced by oxidized low-density lipoprotein via modulating caspase-3 and Bcl-2. Mol Med Rep 17: 6835-6839, 2018.
25. Chen S, Wang Z, Zhou H, He B, Hu D and Jiang H: Icariin reduces high glucose-induced endothelial progenitor cell dysfunction via inhibiting the p38/CREB pathway and activating the Akt/eNOS/NO pathway. Exp Ther Med 18: 4774-4780, 2019.
26. Xiao HB, Liu ZK, Lu XY, Deng CN and Luo ZF: Icariin regulates PRMT/ADMA/DDAH pathway to improve endothelial function. Pharmacol Rep 67: 1147-1154, 2015.
27. Wang FY, Jia J, Song HH, Jia CM, Chen CB and Ma J: Icariin protects vascular endothelial cells from oxidative stress through inhibiting endoplasmic reticulum stress. J Integr Med 17: 205-212, 2019.